Three-Dimensional Dynamics of Collisionless Magnetic Reconnection in Large-Scale Pair Plasmas

L. Yin,[1] W. Daughton,[1] H. Karimabadi,[2] B. J. Albright,[1] Kevin J. Bowers,[1,*] and J. Margulies[1]

[1]*Los Alamos National Laboratory, Los Alamos, New Mexico 87544, USA*

[2]*University of California, San Diego, La Jolla, California 92093, USA*

(Received 1 February 2008; published 15 September 2008)

Using the largest three-dimensional particle-in-cell simulations to date, collisionless magnetic reconnection in large-scale electron-positron plasmas without a guide field is shown to involve complex interaction of tearing and kink modes. The reconnection onset is patchy and occurs at multiple sites which self-organize to form a single, large diffusion region. The diffusion region tends to elongate in the outflow direction and become unstable to secondary kinking and formation of ''plasmoid-rope'' structures with finite extent in the current direction. The secondary kink folds the reconnection current layer, while plasmoid ropes at times follow the folding of the current layer. The interplay between these secondary instabilities plays a key role in controlling the time-dependent reconnection rate in large-scale systems.

DOI: 10.1103/PhysRevLett.101.125001 PACS numbers: 52.35.Vd, 52.27.Ep, 52.35.Py, 52.65.Rr

Collisionless magnetic reconnection is a basic plasma process in which magnetic energy converts rapidly into particle kinetic energy. This process is widely hypothesized to play an important role in a variety of applications, including planetary magnetospheres, solar flares, laboratory fusion machines, and astrophysical settings involving electron-ion and electron-positron (pair) plasmas. Previous reconnection studies of relativistic pair plasmas have examined issues relating to the reconnection rate within fluid models [1] and kinetic simulations focused primarily on particle acceleration by plasma instabilities [2]. In the nonrelativistic limit, recent two-dimensional (2D) work has focused on the physical mechanism for fast reconnection using two-fluid [3] and fully kinetic simulation [4]. However, the typical system size ($\sim$25 inertial lengths) in these particle-in-cell (PIC) simulations was quite small in comparison to the characteristic scales for most astrophysical systems. It is important to understand how the reconnection dynamics scale to larger systems of physical relevance. A recent scaling study using 2D kinetic simulations [5] up to $\sim 1000 d_i$ (where $d_i = c/\omega_{pi}$ is the inertial length) demonstrated a basic tendency to form highly elongated current sheets within the diffusion region. These current sheets are unstable to the cyclical formation of secondary magnetic islands (or plasmoids) and lead to a time-modulated reconnection rate. The average reconnection rate remains fast (inflow velocity $\sim$0.1 Alfvén speed) and is insensitive to system size for large ($\geq 500 d_i$) systems. However, the 2D approximation is questionable since the current aligned drift-kink instability [6] has a growth rate that is typically somewhat larger than tearing (a factor of $\sim 1.7\times$ in this study). While the interaction between these two instabilities has been considered in small-scale simulations [2], the influence on the large-scale evolution remains unexplored due to the computational difficulty of resolving a sufficient number of modes in each direction.

In this work, we examine reconnection dynamics in pair plasmas using the largest 3D PIC simulations to date, a factor of $300\times$ larger than other recent studies [2]. These simulations are large enough to allow the elongation of the diffusion region in the tearing direction and to accommodate 2–20 wavelengths of the fastest growing kink mode. The focus of this work is the nonrelativistic regime from which the essential 3D reconnection dynamics can be compared with 2D results. The highly optimized 3D PIC code VPIC [7] is used to examine reconnection dynamics in a neutral sheet. It is demonstrated that, as the system size becomes large enough ($\gtrsim$100 inertial lengths in the current direction), reconnection onset is patchy and occurs at multiple sites which tend to self-organize to form an elongated diffusion region, as in 2D. The dynamic evolution of the thin current layer and the reconnection rate are controlled by two types of secondary instabilities: (1) secondary kinking which folds the current layer and leads to detached current tubes and (2) formation of plasmoids which have a magnetic field component and a finite extent in the current direction. We refer to these structures as *plasmoid ropes*.

The simulations are initialized with a Harris equilibrium with magnetic field $B_y = B_0 \tanh(x/L)$ and density $n = n_0 \mathrm{sech}^2(x/L)$ provided by drifting Maxwellian distributions with uniform temperature T_e and T_i (L is the half thickness of the current sheet and B_0 is the asymptotic field; drift and current are in the z direction; subscript i denotes positron quantities). A uniform background density n_b consisting of the same temperature but nondrifting plasma is also included. The simulation parameters are $L/d_i = 0.7$, $T_i/T_e = 1$, $\omega_p/\Omega_c = 4$, and $n_b/n_0 = 0.3$ [where $d_i = c/\omega_p$, $\omega_p = \sqrt{(4\pi n_0 e^2)/m_i}$, and $\Omega_c = eB_0/(m_i c)$ are the positron inertial length, plasma frequency, and cyclotron frequency, respectively], as in Ref. [5]. Periodic boundaries are used in y and z with conducting boundaries in x.

In antiparallel geometry, nonlocal linear Vlasov theory predicts [6] two modes: tearing, with wave vectors along y, and kink, along z. Theory predicts that the fastest growing tearing mode has wave number $k_y L = 0.5$ and growth rate $\gamma/\Omega_c = 0.143$, while the fastest growing kink mode has $k_z L = 0.44$ and $\gamma/\Omega_c = 0.25$ (the instabilities grow from noise instead of from an initial perturbation). For a fixed size in the tearing direction, the size of the simulation in the current direction determines the spectrum of linearly unstable kink modes. To examine how the dynamic evolution of the reconnection layer may be influenced by linear and nonlinear competition between the two modes, we use three simulations with fixed size in the tearing plane $200d_i \times 200d_i$ but different sizes $20d_i$, $50d_i$, and $200d_i$ in z to control the allowed spectrum of kink modes (2, 5, and 20 modes, respectively). These simulations follow the dynamics of 16×10^9, 43×10^9, and 172×10^9 particles on a $1000 \times 1000 \times 100$, $1024 \times 1024 \times 256$, and 1024^3 mesh, respectively (for the two largest runs, the cell size is $1.56\lambda_D$, where λ_D is the Debye length, and the time step is $t\Omega_c = 2.79 \times 10^{-2}$).

In 3D, the growth of the initial kink modes saturates around $t\Omega_c \sim 40$ leading to a somewhat broader current layer. As the initial kink modes interact with the slower growing tearing modes, complicated 3D structures emerge throughout the simulation, as shown by the simulation movie [8]. The magnetic islands formed from the tearing instability coalesce to a larger scale leading to the formation of a dominant reconnection site through which most of the magnetic flux is processed. This dominant diffusion region expands in y to form a highly elongated current sheet unstable to secondary kink instability and plasmoid formation. We use results from the small simulation at a late time to illustrate the detailed structure of the elongated diffusion region in the presence of these secondary instabilities. The top panel in Fig. 1 shows an isosurface of weak magnetic field $|B|$ (an approximate null surface) with color indicating current density $|J|$. Intersecting the isosurface is a cutting plane in (x, y) with contours of $|J|$ at a z location near the boundary, indicating the elongated diffusion region along y between the large magnetic islands. Folding of the diffusion region from the secondary kink is shown together with a thin, intense current density ribbon associated with the formation of secondary islands. However, unlike in 2D, where the islands are invariant in the out-of-plane direction, these islands have a helical structure in 3D with a variable radius and finite extent in z as shown in the lower panel (note that the axes are oriented differently in the two panels). These plasmoid ropes have a magnetic field component in z, and the magnetic field follows the bending current ribbon. With the diffusion region highly folded at this time, the inflow is disrupted and reconnection rate is reduced. The evolution of the reconnection layer during time $t\Omega_c = 303 - 556$ is captured in three simulation movies [8] shown from top, bottom, and side views. Prior to folding, the diffusion region undulates from the

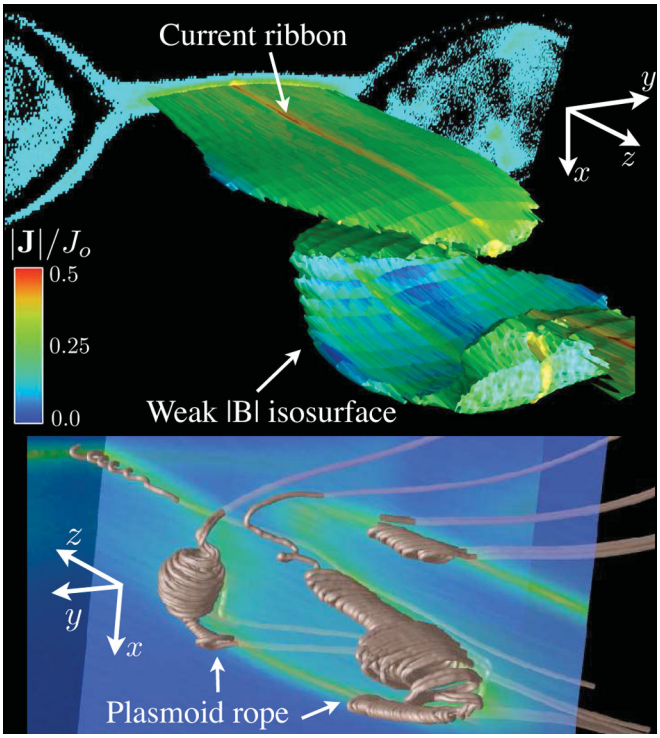

FIG. 1 (color). The diffusion region current sheet for the smallest run at $t\Omega_c = 342$ shows the interaction between the secondary kink and plasmoid formation. The upper panel shows a weak $|B|$ isosurface colored with $|J|$. The diffusion region is folded from the secondary kink with an intense current filament indicating the formation of a plasmoid. In the lower panel, the magnetic field structure associated with this plasmoid rope follows the folding and the current filament.

onset of the secondary kink. Around $t\Omega_c = 353$ (simulation step 12 354 in the movies), folding evolves to a complete roll-up of the current layer and the weak $|B|$ isosurface evolves into two parts: (1) a detached cylindrical tube of current and (2) a relatively flat current sheet that extends over the entire z domain. There is a strong vortex flow around the detached current tube, and the resulting magnetic field is rolled up into a coiled torus structure localized about the ribbon of high current density. This coiled magnetic field is the evolved state of the plasmoid ropes in the lower panel in Fig. 1. This detached current tube eventually recombines with the reformed current layer, and the reconnection rate increases as the inflow is reestablished. During this simulation, the folding and plasmoid-rope formation occurs twice before the system saturates due to the periodic boundaries. The secondary kink and formation of plasmoid ropes play the same key role in controlling the dynamics of the reconnection layer in all three 3D simulations.

However, as the simulation domain in the z direction becomes large enough ($\gtrsim 100d_i$), reconnection onset becomes patchy and occurs at multiple sites, as shown in supplemental Fig. 1 [8]. These sites then self-organize along the z direction to form a single, elongated diffusion

region, as shown by the top panel in Fig. 2. Unlike the two smaller 3D cases, where the diffusion region expands to encompass the entire z domain (see supplemental Fig. 2), the diffusion region in the largest run remains localized with significant inflow occurring between $z/d_i = 30 \rightarrow 120$. Within this region, the characteristic wavelength of the secondary kink instability $\sim 20d_i$ is comparable to the smaller two runs. The reconnection inflow affects the nonlinear evolution of the secondary kink and the thickness of the layer in the diffusion region. As a result, the current layer thickness has spatial dependence, as shown in the lower frame in Fig. 2 by color contours of current density $|J(x, z)|$ at the fixed y position indicated. The thickness of the elongated reconnection layer at the location of the cut indicated by the dashed line in the lower frame is $\sim 3.8d_i$ (full width at half maximum), as estimated from the profile of $|J(x)|$ at the cut shown on the right. This thickness in 3D is comparable to that in 2D, $\sim 3d_i$. On the other hand, the thickness of the current sheet outside the localized, elongated diffusion region is much larger, as seen in the region near the two z boundaries in the lower frame, resulting from the nonlinear saturation of the initial kink modes. As discussed earlier, the highly folded diffusion region current sheet often leads to detached current tubes with intense vortex flow as illustrated in the lower frame.

To quantitatively compare the rate of energy conversion, a total energy diagnostic is shown in the top panel in Fig. 3. For all cases in this study, $\sim 20\%$ of initial magnetic energy is converted to particle kinetic energy over similar time scales. The conversion rate is somewhat slower in the largest 3D simulation, likely due to the finite extent of the reconnection site in z as illustrated in Fig. 2. In the two smaller 3D cases, the diffusion region expands to encompass the entire domain in z well before final saturation. The relatively small differences in overall energy conversion obscure a number of interesting features in the time dependence. Because of the complicated 3D dynamics and multiple reconnection sites, we follow the basic approach outlined in Ref. [5] to compute the reconnection inflow upstream from the dominant reconnection site. The coalescence of tearing islands eventually leads to a single dominant reconnection site for $t\Omega_c > 200$ through which most of the magnetic flux is eventually processed. To estimate a reconnection rate, we imagine a control volume centered about this dominant reconnection site and measure the rate of magnetic flux convected into this region from the inflow. Normalizing this ideal inflow by the local Alfvén speed, the dimensionless reconnection rate is $E_R = c\langle E_z/(BV_A)\rangle$, where $\langle\,\rangle$ represents an average over the inflow surface $V_A = B/(8\pi nm)^{1/2}$ and the electron density n and magnetic field B are measured at the inflow surface. The inflow surface is $\pm 20d_i$ upstream from the dominant diffusion region and has an extent of $8d_i$ in y. For the two smaller 3D cases the control volume extends the entire length in z, while for the largest case the control volume is over the region shown in Fig. 2 where reconnection is active. As illustrated in the bottom panel in Fig. 3, the inflow rate shows a pronounced increase when a dominant diffusion region forms around $t\Omega_c = 200$ (the diagnostic is meaningful only after this time since inflow is measured upstream of this location). Although the evolution is highly

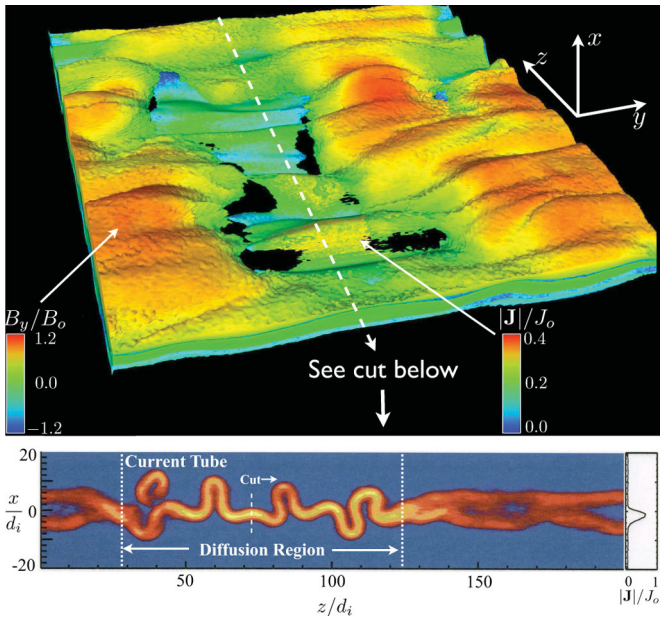

FIG. 2 (color). Characteristic structure of the reconnection layer at late time $t\Omega_c = 289$ for the largest simulation. The upper panel is the superposition of two separate isosurfaces: (1) Magnetic islands are visualized with a constant density isosurface colored by B_y and (2) the diffusion region is visualized with a weak $|B|$ isosurface colored by $|J|$. The detailed structure of $|J(x, z)|$ is shown in the bottom panel by a cutting plane at fixed y (indicated) at time $t\Omega_c = 328$.

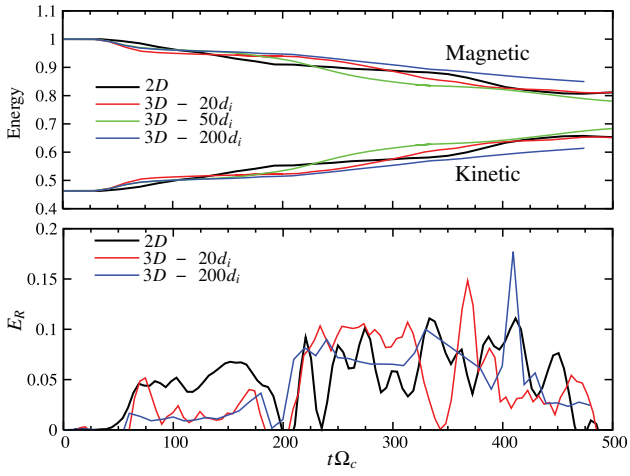

FIG. 3 (color). Time evolution of energy conversion (top) and inflow reconnection rate (bottom: rate for the medium size run is omitted to improve readability; time averages for all cases are given in the text). Magnetic and kinetic energy in the top panel are normalized to the total initial magnetic energy. The inflow reconnection rate diagnostic is meaningful only after a dominant diffusion region has formed $t\Omega_c > 200$ and before recirculation effects dominate $t\Omega_c < 400$.

dynamic in all cases, the underlying dynamics have important differences. In 2D, the large variations in rate correspond to formation and ejection of plasmoids. While in 3D plasmoids are still produced, the highly folded diffusion region from the secondary kink also leads to large variations in the reconnection process. For example, in the small $20d_i$ case, the pronounced decrease in reconnection inflow rate around $t\Omega_c = 342$ is caused by a temporary disruption in the inflow from the folding of the layer illustrated in Fig. 1 and the formation of a current tube thereafter. This feature is less dramatic in the larger run since these blockages have finite extent in z corresponding to the kink wavelength while the inflow rate represents an average over the entire control volume. During $t\Omega_c = 200 \rightarrow 400$, reconnection proceeds through a single dominant diffusion region and the time-averaged reconnection rates are comparable, with $\langle E_R \rangle \approx 0.061$ for 2D, $\langle E_R \rangle \approx 0.073$ for the $20d_i$ 3D case, $\langle E_R \rangle \approx 0.081$ for the $50d_i$ 3D case, and $\langle E_R \rangle \approx 0.067$ for the $200d_i$ 3D case. Taking into account the different normalization factors, these time-averaged reconnection rates are within 10% of the peak rates reported in smaller 2D pair plasmas [4]. This result is potentially an important clue, but one should be cautious since large differences exist in the underlying dynamics. From our initial examinations of the force balance, it is clear that the off-diagonal terms in the electron and positron pressure tensors play a dominant role [4] in balancing the reconnection electric field for both 2D and 3D. However, the physics responsible for controlling the length of the layer may still be quite different. In particular, this Letter has demonstrated that the dynamical evolution of the diffusion region current sheet is dramatically different in 3D due to the presence of secondary kinking, which in turn couples to plasmoid formation in a nontrivial manner. These results suggest that the average reconnection rate by itself is a poor measure of progress towards understanding the physics, since very different dynamics can produce similar average rates. Furthermore, these initial 3D simulations used periodic boundary conditions with fixed system size in the tearing plane; thus, it is premature to make firm conclusions regarding scaling of the reconnection rate in large 3D systems.

We have shown for the first time the complicated 3D reconnection dynamics in a large-scale pair plasma from first-principles kinetic simulations. In agreement with previous 2D simulations, magnetic islands tend to coalesce to a larger scale and elongated current sheets form within the diffusion regions. The main new results in 3D are (1) reconnection onset is patchy in both the y and z directions due to the complex interaction of kink and tearing modes within the initial current sheet; (2) the initial reconnection sites have finite extent in the direction of the current but gradually self-organize in the current direction to form a large diffusion region; (3) the resulting thin current sheet within the diffusion region is unstable to both secondary kink modes and plasmoid-rope formation; (4) the secondary kink leads to a highly folded current sheet from which detached current tubes form together with a new elongated current layer; (5) the cyclic formation of the elongated reconnection layer and the secondary kink as well as formation of plasmoid ropes results in a time-dependent reconnection rate. We have also examined the effect of the guide field and will report in detail elsewhere. Initial results with an intermediate guide field ($0.5B_0$) indicate that the initial kink mode growth rates are smaller ($\gamma/\Omega_c \approx 0.2$) and secondary kink still occurs but does not fold the reconnection layer. However, kink modes are stable in the strong guide field case (B_0); instead, oblique tearing modes are present. These results suggest that reconnection is generally time-dependent and ultimately tied to the dynamics of the secondary instabilities in the elongated current layer. To properly address the time-asymptotic state, open boundary conditions [9] will be used in the future to eliminate recirculation.

Although this work focuses on pair plasma, it has important implications for hydrogen plasma, where the drift-kink mode is replaced by the ion-ion kink mode [6]; the latter, along with lower hybrid drift instability and other current aligned instabilities, may play a similar role in folding the reconnection layer. The resulting complex 3D structure of the diffusion region poses a serious challenge for interpreting spacecraft data.

This work was done under the auspices of the U.S. DOE by LANS LLC LANL and supported by NASA (NNH04AB221), DOE (DE-FG02-06ER54893), and IGPP. Calculations were run on the Roadrunner supercomputer.

*Guest scientist. Present address: D. E. Shaw Research, LLC, New York, NY 10036, USA.

[1] E. G. Blackman and G. B. Field, Phys. Rev. Lett. **72**, 494 (1994); M. Lyutikov and D. Uzdensky, Astrophys. J. **589**, 893 (2003), and references therein.

[2] C. H. Jaroschek, R. A. Treumann, H. Lesch, and M. Scholer, Phys. Plasmas **11**, 1151 (2004); S. Zenitani and M. Hoshino, Astrophys. J. **618**, L111 (2005); **670**, 702 (2007), and references therein.

[3] L. Chacón, Andrei Simakov, V. S. Lukin, and A. Zocco, Phys. Rev. Lett. **101**, 025003 (2008).

[4] N. Bessho and A. Bhattacharjee, Phys. Rev. Lett. **95**, 245001 (2005).

[5] W. Daughton and H. Karimabadi, Phys. Plasmas **14**, 072303 (2007).

[6] W. Daughton, Phys. Plasmas **6**, 1329 (1999).

[7] K. J. Bowers, B. J. Albright *et al.*, Phys. Plasmas **15**, 055703 (2008).

[8] See EPAPS Document No. E-PRLTAO-101-022838 for supplemental figures and movies. For more information on EPAPS, see http://www.aip.org/pubservs/epaps.html.

[9] W. Daughton, J. Scudder, and H. Karimabadi, Phys. Plasmas **13**, 072101 (2006).